Indian Journal of Engineering & Materials Sciences
Vol. 32, December 2025, pp. 808-823
DOI: 10.56042/ijems.v32i06.19171

Enhancing CFRP machining performance: A hybrid fuzzy AHP-Grey relational analysis for parameter optimization

Amit Patil[a*], Kiran Bhole[b], Deepak Singh[b], Sushil Ingle[a] & Rohit Patel[c]

[a]Department of Mechanical Engineering, Bhujbal Knowledge City, MET's Institute of Engineering, Adgaon 422 003, Nashik, India
[b]Department of Mechanical Engineering, Bhartiya Vidya Bhavan's Sardar Patel College of Engineering, Andheri 400 058, Mumbai, India
[c]Department of Mechanical Engineering, Clemson University, Clemson, SC 29634, United States

Received: 27 April 2025; accepted: 11 October 2025

Carbon fiber-reinforced polymers (CFRPs) have become critical materials in aerospace and automotive industries due to their outstanding strength-to-weight ratio. However, their abrasive characteristics have made machining particularly challenging. In this study, a novel hybrid Fuzzy AHP-GRA method has been introduced to optimize CFRP turning parameters—namely, cutting speed, depth of cut, and feed rate. Experiments have been conducted using an L9 orthogonal array with PVD-TiAlN-coated carbide inserts and a water-miscible coolant. The results have indicated that cutting speed (100 m/min) and depth of cut (0.1 mm) have been the most significant factors affecting tool wear and surface finish. While higher cutting speeds have enhanced material removal rates, they have also increased tool wear due to elevated temperatures. Similarly, greater depths of cut have intensified cutting forces and led to more frequent tool chipping. The optimal parameter setting determined by grey relational analysis (100 m/min, 0.1 mm depth of cut, 0.1 mm/rev feed rate) has reduced average flank wear by 2.77% and slightly improved average crater wear by 1.19%, while also yielding superior taper wall finish and cylindrical surface quality (improvements of 16.09% and 9.26%, respectively) compared to the controlled parameter setting (100 m/min, 0.1 mm, 0.3 mm/rev). This data-driven approach has effectively balanced productivity and tool longevity, thereby addressing key industrial challenges in CFRP machining

Keywords: Carbon fibre-reinforced polymer, Fuzzy-AHP-GRA, Optimization, Turning

1 Introduction

Carbon fiber-reinforced polymers (CFRP) have emerged as indispensable materials for various high-performance applications, primarily owing to their exceptional strength-to-weight ratio, high stiffness, and inherent resistance to corrosion[1]. These composites, typically comprising carbon fibers embedded within a polymer matrix such as epoxy, polyester, vinyl ester, or nylon, exhibit anisotropic and heterogeneous microstructures, presenting unique challenges in machining operations[1]. The aerospace, automotive, and sports industries increasingly favour CFRPs over traditional metallic alloys owing to the continuous demand for lightweight construction materials with enhanced mechanical properties. The inherent properties of CFRPs, including their high tensile strength, rigidity, customizable nature, and excellent fatigue resistance, make them suitable for a wide range of engineering applications, including civil engineering projects such as bridge construction, structural reinforcement, and the creation of lightweight and resilient components[2]. These materials, known for their remarkable strength-to-weight ratio, superior stiffness, and resistance to corrosion, are being increasingly utilized in industries that require high-performance materials[3,4]. However, the heterogeneous and abrasive nature of carbon fibers makes machining CFRP composites significantly more complex than machining conventional metal alloys[5,6]. Understanding the metallurgy and behavior of CFRPs is crucial for optimizing manufacturing processes and ensuring the quality and reliability of the finished components[7].

CFRP turning is inherently complex owing to its heterogeneous fiber–matrix structure. Delamination, thermal degradation, and fiber pull-out significantly compromise turning quality and structural integrity[1,8]. Extensive research[5,9–11] has focused on understanding how machining parameters such as cutting speed, feed rate, and depth of cut affect outcomes such as surface roughness, thrust force, and tool wear.

Demir *et al.*[2] analyzed the effects of the tool approach angle, feed rate, and spindle speed on the shape of the chip and surface quality. Yılmaz *et al.*[3] studied the machinability of CFRP pipes with

*Corresponding author (E-mail:amitpatil36@hotmail.com)

different fiber orientations, further emphasizing the impact of material anisotropy on drilling performance.

Despite these contributions, many studies[3,8,9,12,13] have focused on single-response optimization or global tool wear indicators without considering the simultaneous impact on multiple interrelated performance metrics. One recent study adopted multi-criteria decision-making techniques to holistically evaluate and optimize CFRP drilling performance. Grey relational analysis (GRA) is used to convert multiple outputs into a unified performance index, the GRG, which facilitates the comparative evaluation of experimental trials[14,15]. Then, combined with the fuzzy analytical hierarchy process (Fuzzy-AHP), it becomes possible to integrate expert judgment into the weighting of criteria, accommodating the uncertainty and subjectivity involved in prioritizing performance objectives[4]. Rob and Srivastava[16] used Taguchi and multi-objective genetic algorithms for CFRP turning, emphasizing cutting force and tool wear. Rajasekaran *et al.*[5] employed fuzzy modelling to predict surface roughness, while Fedai[17] demonstrated the effectiveness of combining Fuzzy-AHP and GRA in drilling natural fiber composites. However, fewstudies have focused on incorporating localized tool wear measures, such as crater and flank wear, along with surface quality metrics, such as taper and cylindrical wall roughness, within a multi-response optimization framework for CFRP turning and milling.

Tool wear is a critical concern in CFRP machining because of the abrasive nature of carbon fibers[8,18]. The abrasive nature of carbon fibers leads to rapid tool wear, necessitating the use of specialized cutting tools and machining strategies. High-speed steel and tungsten carbide tools constitute approximately 97% of the materials used for cutting composite materials[1,12]. Diamond coatings and advanced tool geometries are often employed to enhance tool life and improve the machining performance[19]. Surface quality is significantly affected by tool wear, with worn tools leading to increased surface roughness, burr formation, and delamination[20]. Maintaining sharp cutting edges is crucial to minimize these defects and achieve the desired surface finish. The complex interplay between the tool wear and surface quality necessitates a comprehensive understanding of the underlying wear mechanisms and their influence on the machining process. The feed rate is a significant factor, and a lower feed per tooth leads to high tool wear and poor surface quality[6]. Efficient management of cutting parameters, such as speed, feed, and depth of cut, is essential for maximizing tool life and minimizing surface damage[21]. The surface quality is also influenced by the cutting parameters, with lower feed rates and optimized cutting speeds typically resulting in smoother surfaces. Achieving the desired surface finish and dimensional accuracy in turned CFRP components requires careful selection of cutting parameters and tool geometries[13].

Previous studies on CFRP machining optimization have failed to develop a robust methodology that simultaneously addresses tool wear and surface finish while accounting for their complex interdependencies. This study bridges this critical gap by proposing the first integrated Fuzzy AHP-GRA framework for multi-objective optimization of turning parameters under industrial coolant conditions. Our systematic approach reveals that conventional parameter selection methods inadequately capture the nonlinear effects of cutting conditions, as demonstrated by the 39.7% increase in flank wear (58-81 μm) and 36.7% increase in crater wear (158-216 μm) when the speed increases from 100 to 140 m/min. Through rigorous Taguchi-designed experiments and grey relational analysis weighted by Fuzzy AHP, we identified the optimal controlled parameter combination (100 m/min cutting speed, 0.1 mm depth of cut, 0.3 mm/rev feed rate) that achieves superior balanced performance, with cutting speed (52.4%) and depth of cut (45.3%) emerging as statistically dominant factors by ANOVA. This represents a significant advancement over single-criterion optimization methods, providing manufacturers with a validated decision-making tool that extends tool life while maintaining surface quality in practical CFRP machining applications. Objectives of present study are:

1. To develop a hybrid Fuzzy AHP-GRA method for optimizing CFRP turning parameters.
2. Determine the best cutting speed, depth of cut, and feed rate, which reduce tool wear and improve the surface finish.
3. To analyse the effect of cutting parameters on tool wear and surface quality through experiments.
4. To provide a practical solution for industries to machine CFRP more efficiently.

1.1 Metallurgical behaviour of CFRP

The metallurgy of CFRPs is fundamentally different from that of traditional metals, because it involves the interaction between two dissimilar materials: carbon fibers and the polymer matrix.

Carbon fibers are characterized by a graphitic structure, which provides high tensile strength and stiffness along the fiber direction. The mechanical properties of CFRPs are highly dependent on the fiber volume fraction, fiber orientation, and interfacial bonding between the fibers and matrix. The matrix material transfers stress between the fibers, protects them from environmental damage, and provides an overall shape and stability to the composite structure[2,22]. The polymer matrix, which binds the carbon fibers together, protects them from environmental factors such as moisture and ultraviolet radiation. When machining CFRPs, the heterogeneous nature of the material leads to non-uniform stress distributions and complex failure mechanisms. The high-strength and abrasive nature of carbon fibers contribute significantly to rapid tool wear, whereas the low thermal conductivity of the polymer matrix can result in localized heat build-up in the cutting zone, leading to thermal degradation of the matrix material[23,24]. The effective machining of CFRPs requires a thorough understanding of these material properties and their influence on the machining process. The use of CFRPs has numerous advantages, including at high strength-to-weight ratio, which enables significant weight reduction in structural components without compromising mechanical integrity. Moreover, CFRPs exhibit excellent fatigue resistance, corrosion resistance, and dimensional stability, making them ideal for use in harsh environments and demanding applications[25–27]. Their high strength-to-weight ratio is a significant benefit, allowing for lighter and more efficient structures than those made from conventional materials such as steel and concrete[27].Another key benefit of CFRPs is their resistance to corrosion, which makes them highly durable under harsh environmental conditions, where metals might degrade over time. CFRPs also offer design flexibility, enabling the creation of complex shapes and geometries that are difficult or impossible to achieve by using traditional materials. However, CFRPs also have certain limitations, including their high initial cost compared with traditional materials, which can be a barrier to their adoption in some applications[15,27]. The initial costs associated with CFRPs are high, as are those associated with specialized manufacturing and repair processes. The lack of standardized design codes and guidelines for CFRP structures can pose challenges for engineers and designers[28]. The low ductility and impact resistance of CFRPs can also be of concern in applications in which these properties are critical. Despite their increasing use, machining CFRPs presents substantial challenges owing to the inherent properties of the material and complex interactions between the cutting tool and workpiece. Tool wear is a significant issue because the abrasive nature of carbon fibers causes rapid degradation of cutting tool edges, leading to increased cutting forces, reduced surface quality, and premature tool failure[2,29]. Achieving the desired surface finish and dimensional accuracy in machined CFRP components can be difficult owing to the anisotropic nature of the material and its susceptibility to damage during machining. The anisotropic nature of CFRPs implies that their properties vary depending on their direction, which can result in uneven material removal and surface inconsistencies during machining. Cutting CFRPs can generate significant heat owing to the poor thermal conductivity of the polymer matrix, which can lead to the thermal degradation of the material and further accelerate tool wear[30]. Delamination, fiber pull-out, and matrix cracking are common defects that can occur during machining, compromising the structural integrity and performance of the finished component[6]. Figure 1 illustrates the challenges and possible solutions to CFRP machining.

2 Materials and Methods

This experiment conducted shearing of CFRP on CNC turning as per the Taguchi-based L9 (3^3) orthogonal array. Each trial was conducted 50 times to observe tool health and surface quality produced under specific process parameter combinations. Accumulated results after processing using the fuzzy-AHP-GRA hybrid approach for optimum setting process parameter identification. Furthermore,

Fig. 1 — Challenges and possible solutions in CFRP machining.

optimum parameter determination and validation were conducted.

2.1 Material

In this turning experiment, a 3K CFRP woven fabric + epoxy resin matrix material with a size of Ø20 × 100 mm was used. The material was made using the compression method, and the surface was finished using a wax matt finish.

Table 1 — Process parameters and their levels.

Parameters	Levels		
	1	2	3
Cutting Spee (m/min)	100	120	140
Depth of Cut (mm)	0.1	0.15	0.25
Feed (mm/rev.)	0.1	0.2	0.3
Coolant	Water miscible 8% concentration at 3 bar		
Cutting Tool	SECO DNMG TS2500 PVD-TiAlN		

Table 2 — Taguchi based L9 (3^3) orthogonal array.

Trial Nos.	Cutting Speed (m/min)	DOC (mm)	Feed (mm/rev.)
1	100	0.1	0.3
2	100	0.15	0.2
3	100	0.25	0.1
4	120	0.1	0.2
5	120	0.15	0.1
6	120	0.25	0.3
7	140	0.1	0.1
8	140	0.15	0.3
9	140	0.25	0.2

2.2 Process parameter set-up

The CFRP turning operations were conducted using a SECO DNMG TS2500PVD-TiAlN coated insert with a nose radius of 0.4 mm. The coolant was water miscible, with an 8% concentration injected at the secondary and tertiary cutting zones through the nozzle at 3 bars. Table 1 lists the shearing parameters and their levels used for conducting the experiment. Furthermore, the Taguchi-based L9 (3^3) orthogonal array (shown in Table 2) design of the experiment was tabulated to examine the contribution of each shearing parameter to performance.

2.3 Experimental set-up

CFRP turning was performed on a 2D CNC lathe machine. Each trial was repeated 50 times to verify the cutting tool performance and test the parametric combination for continuous production purposes. After each batch of the respective trial cycle, the coolant and insert were changed to justify the orthogonal array. The experimental details are shown in Fig. 2.

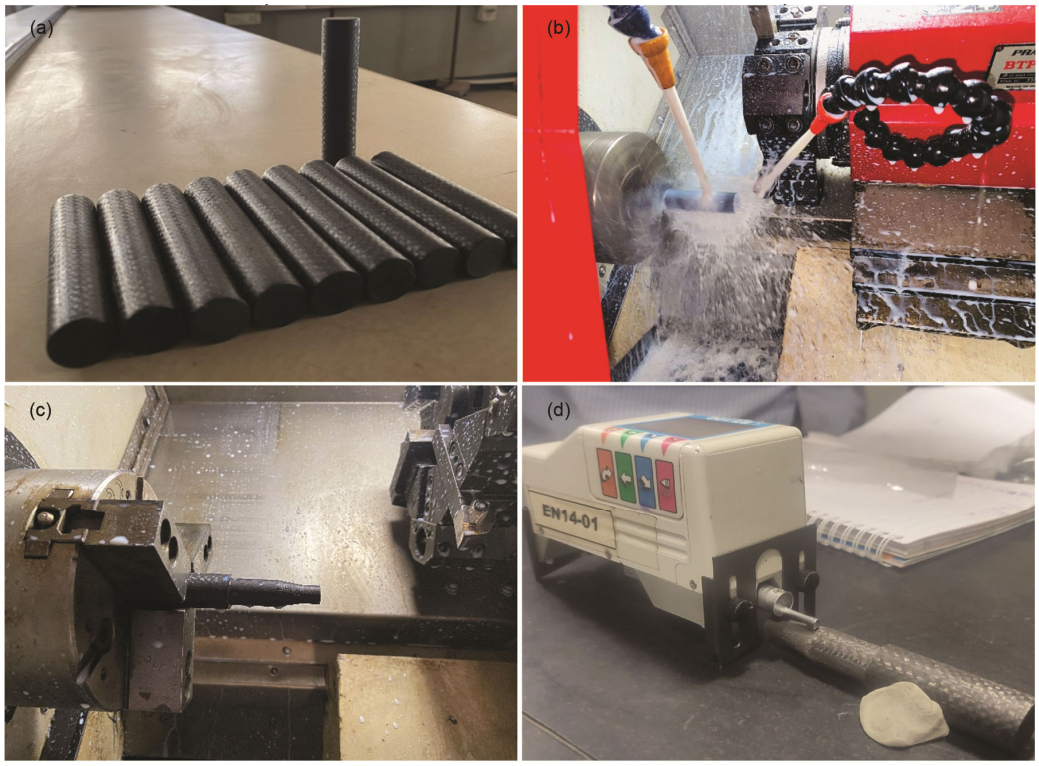

Fig. 2 — (a) 3K CFRP material (HSN CODE-68151200, (b) Turning of CFRP under 3 bar coolant pressure, (c) Finished Component and (d) Measuring the surface texture (Ra).

2.4 Methodology

The prime objective of this experiment was to define a set of process parameters for obtaining consistent surface quality at a higher tool life. The CFRP turning results of the L9 array trials were measured in terms of Crater, Flank wear using scanning electron microscopy. The important aspect is that the surface texture is carried out on a ZEISS SURFCON 130A at a 5 mm cut off length on the tapered and cylindrical surface of the turned surface. The performance of the experiments is summarized in Table 3.

To determine the optimum set of process parameters based on weights provided by an expert in the domain and optimum setting parameters for the desired performance in CFRP turning, the following prescribed flow was deployed in this study (shown in Fig. 3).

2.5 Fuzzy-AHP-Grey relational analysis

In study, the Fuzzy-AHP-Grey relational hybrid approach was used to determine the optimum parameter set.Fuzzy AHP, using the geometric mean method, handles multi-criteria decision-making with inherent uncertainty using fuzzy numbers to represent the importance of criteria. This method aids in maintaining consistency and reducing the effects of extreme values[31–34]. Grey relational analysis was then

Table 3 — Performance of the experimental trials.

Trial No.	Avg. Flank Wear (µm)	Avg. Crater Wear (µm)	Avg. Taper Wall Finish (µm)	Avg. Cylindrical Wall Finish (µm)
1	51.52	128.587	2.361	1.824
2	58.034	166	2.657	2.701
3	63.906	179.254	4.436	1.147
4	58.549	156.828	3.509	1.147
5	66.483	157.175	4.911	2.471
6	77.919	239.905	5.496	2.722
7	68.416	185.554	4.614	1.587
8	84.523	196.703	3.499	4.082
9	89.374	265.384	9.258	13.76

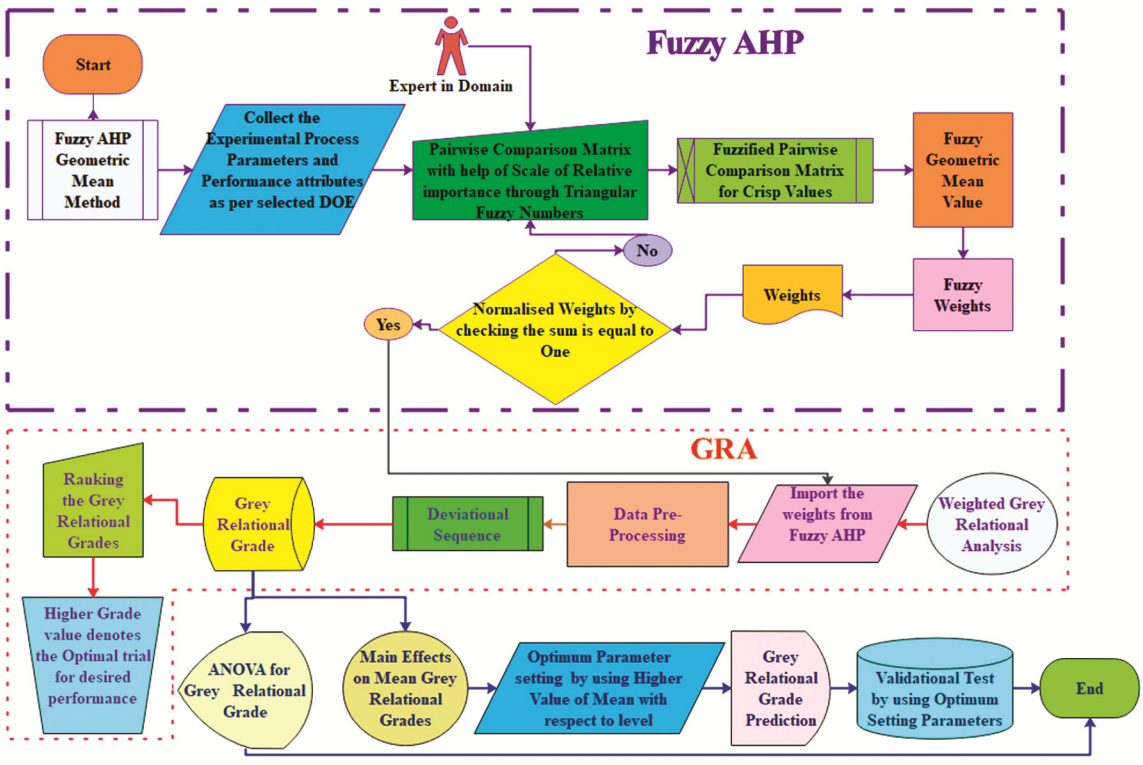

Fig. 3 — Fuzzy-AHP-GRA process and optimum setting parameter flow chart.

used with the normalized fuzzy AHP weights to determine the optimal controlled parameter.

GRA is particularly useful for evaluating relationships in systems with limited information and for identifying the most suitable solution by comparing a data series to an ideal reference series[35–38]. The Fuzzy-AHP-Grey relational hybrid approach procedure is described in the following steps[31,32,39–41].

2.5.1 Fuzzy AHP (Geometric mean method)

Step 1: Pairwise comparison matrix

A pairwise comparison matrix was created based on a single decision-maker's assessment of criteria importance, utilizing a relative importance scale with triangular fuzzy numbers (see Table 4). The resulting pairwise comparison matrices are presented in Table 5.

Step 2: Fuzzifiedpair wise comparison matrix (Ã) for crisp values

The pairwise comparison matrix was transformed into a fuzzified matrix using triangular fuzzy numbers. Each entry in the matrix was replaced with a triplet representing the least value (l), mean value (m), and maximum value (u) of the fuzzy number. This fuzzified matrix was obtained using Equation (1). The Fuzzified pairwise comparison matrix using equation (1) and (2) is illustrated in Table 6. Equation (2) was used for the reciprocal crisp values to convert them into triangular fuzzy numbers.

$$\tilde{A} = \begin{bmatrix} 1 & \tilde{a}_{12} & \cdots & \tilde{a}_{1n} \\ \tilde{a}_{21} & 1 & \ldots & \tilde{a}_{2n} \\ \vdots & \vdots & \ddots & \vdots \\ \tilde{a}_{n1} & \tilde{a}_{n2} & \cdots & 1 \end{bmatrix} \quad \ldots(1)$$

$$\tilde{A}^{-1} = (l, m, u)^{-1} = \left(\frac{1}{u}, \frac{1}{m}, \frac{1}{l}\right) \quad \ldots(2)$$

Step 3: Fuzzy geometric mean value

The Fuzzy Geometric Mean ($\tilde{r}$) was calculated using equation (3). Table 7 presents the calculated fuzzy geometric mean values for each criterion.

$$\tilde{r} = [(l_1, m_1, u_1) \otimes (l_2, m_2, u_2) \otimes (l_3, m_3, u_3) \otimes l4{,}m4{,}u4 \otimes l4{,}m4{,}u41 \text{No. of Criteria} \quad \ldots(3)$$

Step 4: Fuzzy weights

These weights were evaluated using Equation (4). First, find and ($\tilde{r}_{iT}$) and then proceed for their inverse ($\tilde{r}_{iT}{}^{-1}$). Furthermore, the values of($\tilde{r}_{iT}$) and ($\tilde{r}_{iT}{}^{-1}$) are given inEquation (4) to obtain the fuzzy weights ($\widetilde{w}_i$)(shown in Table 8).

$$\widetilde{w}_i = \tilde{r}_{iT} \otimes (\tilde{r}_1 \oplus \tilde{r}_2 \oplus \tilde{r}_3 \oplus \ldots\ldots \oplus \tilde{r}_n)^{(-1)}$$

here,

$$(\tilde{r}_{iT}) = (\tilde{r}_1 \oplus \tilde{r}_2 \oplus \tilde{r}_3 \oplus \tilde{r}_4) \quad \ldots(4)$$

Step 55 Weights

In this step, the fuzzy weights are de-fuzzified using the center of the area in Equation (5). Next, we check the de-fuzzified weights for the normalization using the criteria illustrated in Table 9

Table 4 — Scale of relative importance[31,42].

Crisp Values	Triangular Fuzzy Number *(l, m, u)*	Relative Importance
1	1, 1, 1	Equal Importance
3	2, 3, 4	Moderate Importance
5	4, 5, 6	Strong Importance
7	6, 7, 8	Very Strong Importance
9	9, 9, 9	Extreme Importance
Intermediate Values		
2	1, 2, 3	
4	3, 4, 5	
6	5, 6, 7	
8	7, 8, 9	

Table 5 — Pairwise comparison matrix.

Criteria	Crater Wear (µm)	Flank Wear (µm)	Taper Wall Finish (µm)	Cylindrical Wall Finish (µm)
Flank Wear (µm)	1	3	2	2
Crater Wear (µm)	1/3	1	2	1
Taper Wall Finish (µm)	1/2	1/2	1	9
Cylindrical Wall Finish (µm)	1/2	1	7	1

Table 6 — Fuzzified pairwise comparison matrix.

Criteria	Crater Wear (µm)	Flank Wear (µm)	Taper Wall Finish (µm)	Cylindrical Wall Finish (µm)
Flank Wear (µm)	1, 1, 1	2, 3, 4	1, 2, 3	1, 2, 3
Crater Wear (µm)	1/4, 1/3, 1/2	1, 1, 1	1, 2, 3	1, 1, 1
Taper Wall Finish (µm)	1/3, 1/2, 1/1	1/3, 1/2, 1/2	1, 1, 1	9, 9, 9
Cylindrical Wall Finish (µm)	1/3, 1/2, 1/1	1, 1, 1	6, 7, 8	1, 1, 1

Table 7 — Fuzzy geometric mean value.

Criteria	Crater Wear (μm)	Flank Wear (μm)	Taper Wall Finish (μm)	Cylindrical Wall Finish (μm)	Fuzzy Geometric Mean Value ($\tilde{r}$)
Flank Wear (μm)	1, 1, 1	2, 3, 4	1, 2, 3	1, 2, 3	(1.189, 1.861, 2.449)
Crater Wear (μm)	1/4, 1/3, 1/2	1, 1, 1	1, 2, 3	1, 1, 1	(0.7071, 0.9036, 1.106)
Taper Wall Finish (μm)	1/3, 1/2, 1/1	1/3, 1/2, 1/2	1, 1, 1	9, 9, 9	(1, 1.224, 1.456)
Cylindrical Wall Finish (μm)	1/3, 1/2, 1/1	1, 1, 1	6, 7, 8	1, 1, 1	(1.189, 1.3677, 1.681)

Table 8 — Fuzzy weights ($\widetilde{w}_i$).

Criteria	Fuzzy Geometric Mean Value ($\tilde{r}$)	Total Fuzzy Geometric Mean Value ($\tilde{r}_{iT}$)	Inverse of Fuzzy Geometric Mean Value ($\tilde{r}_{iT}{}^{-1}$)	Fuzzy Weights ($\widetilde{w}_i$)
Flank Wear (μm)	(1.189, 1.861, 2.449)	4.085, 5.356, 6.692	0.149, 0.186, 0.244	0.177, 0.347, 0.599
Crater Wear (μm)	(0.707, 0.903, 1.106)			0.105, 0.168, 0.270
Taper Wall Finish (μm)	(1, 1.224, 1.456)			0.149, 0.228, 0.356
Cylindrical Wall Finish (μm)	(1.189, 1.367, 1.681)			(0.177, 0.255, 0.411

Table 9 — Weights.

Criteria	Fuzzy Weights ($\widetilde{w}_i$)	De-fuzzified Weight (w_i)
Flank Wear (μm)	0.1771, 0.3472, 0.5992	0.3745
Crater Wear (μm)	0.1053, 0.1686, 0.2706	0.1815
Taper Wall Finish (μm)	0.149, 0.228, 0.3562	0.2444
Cylindrical Wall Finish (μm)	0.1771, 0.2552, 0.4113	0.2812
Total (w_{iT})		1.0816

Table 10 — Normalised weights.

Criteria	$\frac{\text{De}-\text{fuzzified Weight } (w_i)}{(w_{iT})}$	Normalized Weight (w_{ni})
Flank Wear (μm)	0.374/1.081	0.346
Crater Wear (μm)	0.181/1.081	0.167
Taper Wall Finish (μm)	0.244/1.081	0.226
Cylindrical Wall Finish (μm)	0.281/1.081	0.26
Total of Normalized Weight (w_{nT})=		1

$$w_i = \left(\frac{l+m+u}{3}\right) \quad ...(5)$$

If Total of De-fuzzified Weight (w_{iT})> 1 then normalisation required. Here, 1.0816 > 1 then normalisation is required.

Step 6: Normalized weights (w_{ni})

Equation (6) was used to obtain the normalized weights, as listed in Table 10. These normalized weights were further moved for grey relational analysis.

$$w_{ni} = \frac{\text{De}-\text{fuzzified Weight } (w_i)}{(w_{iT})} \quad ...(6)$$

If Total of Normalized Weight (w_{nT}) = 1.00 ……. Acceptable, otherwise not acceptable

2.5.2 Grey relational analysis

Step 7: Pre-processing of experimental outputs

The Minimum and maximum values were determined from the experimental responses to establish the weights for each response attribute[1,11,13,20]. Table 11 lists the details of the minimum, maximum, and assigned weights of each attribute.

Step 8: Normalization by specific criteria

Linear normalization is performed based on whether the characteristic is beneficial or non-beneficial using Equations (7) and (8), respectively. Table 12 lists the normalized criteria.

$$x_i^*(k) = \frac{x_i^o(k) - \min x_i^o(k)}{\max x_i^o(k) - \min x_i^o(k)} \; For\ Beneficial\ criteria \quad ...(7)$$

$$x_i^*(k) = \frac{\max x_i^o(k) - x_i^o(k)}{\max x_i^o(k) - \min x_i^o(k)} \; ...For\ non-Beneficial\ criteria \quad (8)$$

Step 9: Deviational sequence

The deviational sequence was obtained using Equation (3). Table 13 presents the deviational sequences of the normalized attributes.

$$[1 - x_i^*] \quad ...(8)$$

Step 10: Grey relational coefficient

Equation (4) was applied to determine the Grey relational coefficient, where, $\triangle_{oi}(k)$is the absolute difference, $\triangle min = 0$ and $\triangle max = 1.\zeta$ is the smaller and distinguished ability is the larger known as distinguished coefficient, generally $\zeta = 0.5$, Following Table 14 depicts the grey relational coefficient ($\xi_i(k)$).

Table 11 — Avg. performance parameters.

Trial Nos.	Avg. Flank Wear (μm)	Avg. Crater Wear (μm)	Avg. Taper Wall Finish (μm)	Avg. Cylindrical Wall Finish (μm)
1	51.52	128.587	2.361	1.824
2	58.034	166	2.657	2.701
3	63.906	179.254	4.436	1.147
4	58.549	156.828	3.509	1.147
5	66.483	157.175	4.911	2.471
6	77.919	239.905	5.496	2.722
7	68.416	185.554	4.614	1.587
8	84.523	196.703	3.499	4.082
9	89.374	265.384	9.258	13.76
MAX	89.374	265.384	9.258	13.76
MIN	51.52	128.587	2.361	1.147
Weights from Fuzzy AHP (w_{ni})	0.346	0.18	0.226	0.26
Criteria	Non-Beneficial	Non-Beneficial	Non-Beneficial	Non-Beneficial

Table 12 — Normalized criteria.

Trial Nos.	Avg. Flank Wear (μm)	Avg. Crater Wear (μm)	Avg. Taper Wall Finish (μm)	Avg. Cylindrical Wall Finish (μm)
1	1	1	1	0.94632522
2	0.82791779	0.72650716	0.9570828	0.876793784
3	0.67279548	0.629619071	0.6991446	1
4	0.81431289	0.793555414	0.8335508	1
5	0.60471813	0.791018809	0.630274	0.895028938
6	0.30261003	0.186254085	0.5454545	0.875128835
7	0.55365351	0.583565429	0.6733362	0.965115357
8	0.12815026	0.502065104	0.8350007	0.767303576
9	0	0	0	0

Table 13 — Deviational sequence of the normalized attributes.

Trial Nos.	Avg. Flank Wear (μm)	Avg. Crater Wear (μm)	Avg. Taper Wall Finish (μm)	Avg. Cylindrical Wall Finish (μm)
1	0	0	0	0.05367478
2	0.17208221	0.27349284	0.0429172	0.123206216
3	0.32720452	0.370380929	0.3008554	0
4	0.18568711	0.206444586	0.1664492	0
5	0.39528187	0.208981191	0.369726	0.104971062
6	0.69738997	0.813745915	0.4545455	0.124871165
7	0.44634649	0.416434571	0.3266638	0.034884643
8	0.87184974	0.497934896	0.1649993	0.232696424
9	1	1	1	1

Table 14 — Grey relational coefficient $\xi_i(k)$).

Trial Nos.	Avg. Flank Wear (μm)	Avg. Crater Wear (μm)	Avg. Taper Wall Finish (μm)	Avg. Cylindrical Wall Finish (μm)
1	1	1	1	0.903057206
2	0.74395661	0.646418395	0.9209507	0.802302653
3	0.60444544	0.574461116	0.6243324	1
4	0.72919556	0.707769597	0.7502448	1
5	0.55848333	0.705237327	0.5748937	0.826485814
6	0.4175749	0.380591098	0.5238095	0.800164943
7	0.52834771	0.545592687	0.6048408	0.934780998
8	0.3644714	0.501034689	0.7518805	0.682410864
9	0.33333333	0.333333333	0.3333333	0.333333333

Table 15 — Grey relational grade ranking.

Trial Nos.	Avg. Flank Wear (µm)	Avg. Crater Wear (µm)	Avg. Taper Wall Finish (µm)	Avg. Cylindrical Wall Finish (µm)	Summation	Grades	Rank
1	1	1	1	0.90305	0.97479	0.2436	1
2	0.7439	0.6464	0.9209	0.8023	0.7827	0.1956	3
3	0.6044	0.5744	0.6243	1	0.7067	0.1766	4
4	0.7291	0.7077	0.7502	1	0.8007	0.2001	2
5	0.5584	0.7052	0.5748	0.8264	0.6564	0.1641	5
6	0.4175	0.3805	0.5238	0.8001	0.5348	0.1337	8
7	0.5283	0.5455	0.6048	0.9347	0.6542	0.1635	6
8	0.3644	0.5010	0.7518	0.6824	0.5576	0.1394	7
9	0.3333	0.3333	0.3333	0.3333	0.3333	0.0833	9

Table 16 — Optimum-controlled process parameters set with performance.

	Process Parameters			Performance Parameters			
Trial No.	Cutting Speed (m/min)	DOC (mm)	Feed (mm/rev.)	Avg. Flank Wear (µm)	Avg. Crater Wear (µm)	Avg. Taper Wall Finish (µm)	Avg. Cylindrical Wall Finish (µm)
1	100	0.1	0.3	51.52	128.587	2.361	1.824

$$\xi_i(k) = \frac{\triangle min + \zeta \triangle max}{\triangle_{oi}(k) + \zeta \triangle max} \zeta \in (0,1) \quad \ldots (10)$$

Step 11: Grey relational grade and rank

Equation (11) defines the grey relational grade γ_i) from the average sum of the Grey Relational coefficients.

$$\gamma_i = \frac{1}{n}\sum_{k=1}^{n}(w_{ni})(k)\xi_i(k) \quad \ldots (11)$$

where w_{ni} denotes the criterion weight. Table 15 shows the grey relational grades of all trials.

Step 12: Optimum set of controlled parameters from gray relational grade

From Table 15, Trial No. 1 indicates a higher value of GRG than the other trials. Therefore, Trial No. 1 had an optimum set of process parameters to satisfy the goal of CFRP turning according to the decided weights. Table 16 shows the optimum controlled process parameter set with the performance.

3 Results and Discussion

The performance of the trial experiment with 50 cycles was measured quantitatively in terms of flank wear, crater wear, and surface quality measured at the cylindrical and taper portions of the component. The quantitative performance values are listed in Table 3. According to the ANOVA Cutting speed and depth of cut are the dominant shearing factors compared with the feed rate in CFRP turning.

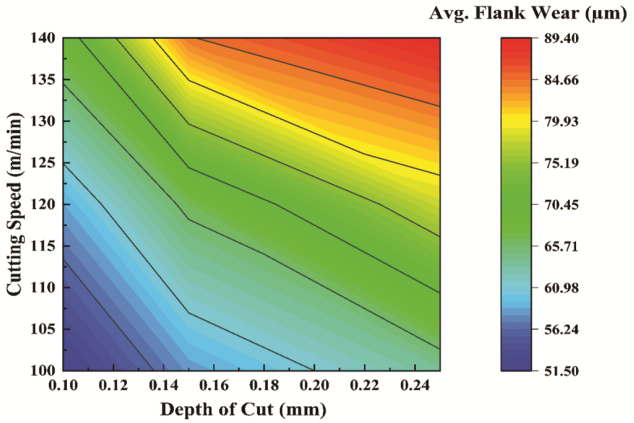

Fig. 4 — Effect of cutting speed and DOC on flank health of cutting insert after 50 component machining.

3.1 Flank wear

Flank wear is the output of the intense friction of the tool insert and workpiece surface in the tertiary machining zone.Abrasive carbon fibers in CFRP contribute significantly to accelerated flank wear, which can lead to poor surface finish and dimensional inaccuracies. Monitoring and controlling flank wear is essential for optimizing the turning process, as excessive wear can result in increased cutting forces, heat generation, and ultimately, tool failure.

Figure 4 illustrates that a lower cutting speed and DOC in CFRP turning produce minimum flank damage compared to a higher cutting speed and DOC. A higher cutting speed increases the frictional heat, and a higher DOC exposes a larger area of the cutting tool to the abrasive nature of the fiber. Therefore, excessive flank wear was observed. Scanning electron micrographs (shown in Fig. 5[b &c])confirm that

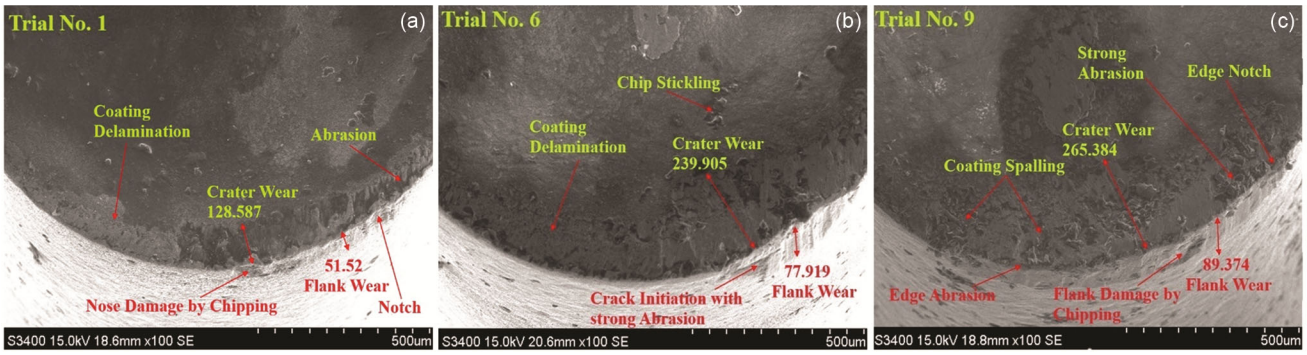

Fig. 5 — Scanning electron micrographs (a) Trial No. 1, (b) Trial No. 6, and (c) Trial No. 9.

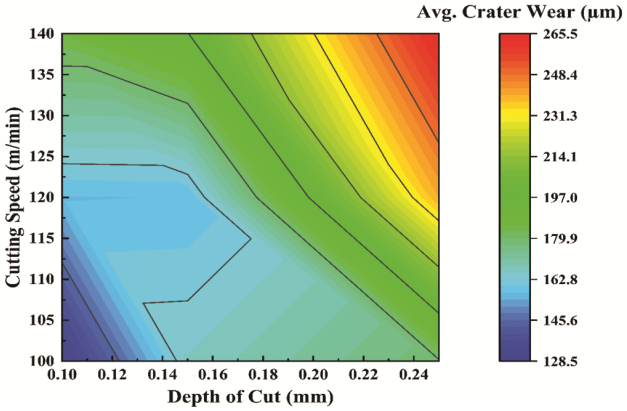

Fig. 6 — Effect of cutting speed and DOC on crater wear of cutting insert after 50 component machining.

higher values of cutting speed and DOC are prone to flank wear with tool life degradation.

Observation of Trial No.1 micrograph at cutting speed100 m/min with 0.1 mm DOC shows much lesser flank damage with abrasion wear among Trials 6 and 9. Trials 6 and 9 had cutting speeds of 120, 140 with 0.25 DOC. The micrographs of Trials 6 and 9 clearly indicate that a higher cutting speed and DOC created coating spalling and edge notches with high rake face wear. The flank face was infected by chipping with wear at 77.919 µm and 89.374 µm in trials 6 and 9, respectively.

3.2 Crater wear

In CFRP turning, the rake face is significantly affected by abrasion wear through fiber chips. The chip flow and its dimensions depend primarily on the cutting speed and DOC. Crater wear is a concave-shaped abrasion caused by the rubbing of the chip surface and tool rake face. Figure 6 clearly indicates that a lower level of cutting speed and DOC results in minimum crater wear. In particular, DOC was more strongly influenced by crater damage than by cutting speed. A higher DOC value creates a thick fiber chip with a large cutting force, and the cutting speed provides velocity for the movement of the emerged chip over the rake face, resulting in the generation of concave-shaped abrasion. Trials 3, 6, and 9 indicate a higher rate of crater wear at 0.25 mm DOC irrespective of cutting speed, as illustrated in Figs (5b, 5c & 7d). Similarly, the scanning electron micrographs of Trials 3, 5, and 7 show an increase in the crater wear value with respect to the applied DOC (shown in Fig. 7). The overall Depth of Cut is sensible for crater damage to support the cutting speed rate.

All micrographs (illustrated in Figs [5 &7]) show the notch and edge damage of the cutting insert caused by sudden impact and strong abrasion, respectively. A higher cutting speed rate generated heat in the secondary and tertiary shearing zones, which propagated the coating delamination of the insert, and the abrasive nature with the strength of the CFRP created chipping at the flank face. Furthermore, the tool experienced catastrophic failure owing to the crack initiation.

The SEM micrographs (refer Figs [5c &7f]) clearly showed the thermal effects at higher cutting speeds, with clear resin smearing and micro-cracking along the fiber-matrix interface. At 140 m/min, the crater area showed signs of thermal degradation, with a softened epoxy matrix spreading across the rake face and covering the fiber edges. This was in line with the measured rise in crater wear (up to 265 µm) and the drop in surface finish (taper wall roughness 9.258 µm, cylindrical finish 13.76 µm). SEM images showed cleaner fiber turning with less resin adhesion at the best speed of 100 m/min. This was in line with lower wear values and smoother surfaces. SEM observations also confirmed that mechanical effects were stronger at deeper cuts. For example, at a depth

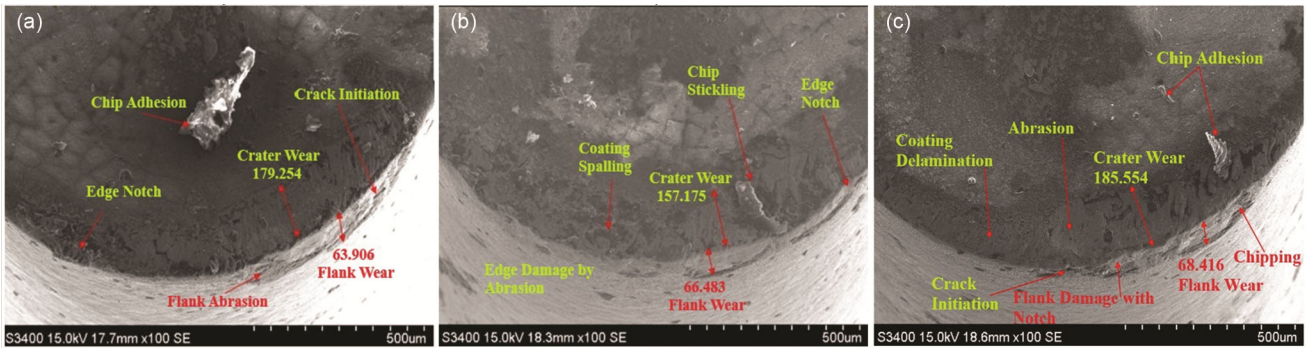

Fig. 7 — Scanning electron micrographs (a) Trial No. 3, (b) Trial No. 5, (c) Trial No. 7.

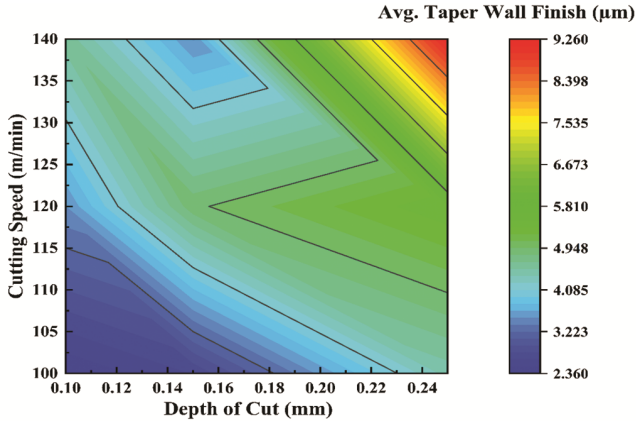

Fig. 8 — Effect of cutting speed and DOC on avg. taper wall finish on components.

of 0.25 mm, the flank wear zone showed severe edge chipping and notch formation, and the machined surface showed fractured fibers and delamination bands. These flaws are why the flank wear was higher (up to 89.3 µm) and the surface integrity was poor in the tests. On the other hand, SEM images (refer Fig. 5a) at a depth of 0.1 mm showed intact fiber bundles with little pull-out and uniform resin removal, which confirmed the better finish and less wear. The SEM evidence shows that both thermal stresses at high speeds and mechanical stresses at greater depths directly speed up tool wear and lower the quality of CFRP surfaces.

3.3 Taper wall finish

Taper in CFRP turning refers to an unintended variation in the diameter of the turned part along its axial length. This can be difficult to shear, because uneven material removal leads to cutting tool wear by abrasion. The anisotropy of CFRP sensitively reacts to the cutting the fiber in its orientation; otherwise, a poor surface finish occurs. The surface plot in Figure 8 shows that a higher value of cutting speed and DOC disturbs the surface texture owing to the effect of tool wear and anisotropy. At higher cutting speeds, the shearing of fiber threads was uneven, resulting in the pull-out and delamination observed in the components turned by Trials 6 and 9 (shown in Figs 9[a & b]). At higher shearing parameter values, CFRP exhibited a poor response in terms of surface quality and dimension stability. The starting edge of the tapered portion is uneven and delaminated by the fiber orientation against the movement of the cutting insert, as depicted in Fig. 9.

3.4 Cylindrical wall finish

The cylindrical wall finish is a general observation technique in the turning operation to determine the prominence of the shearing parameters. In this study, the average cylindrical wall finish was measured after 50 cycles for each trial. Figure 10 portrayed that, only cutting speed 140 m/min and DOC 0.15 and 0.25 in Trial 8 and 9 respectively illustrated poorest surface texture among other trials.In Trial 1, at a lower cutting speed of 100 m/min with a 0.1 mm DOC, the desirable Avg. surface quality (Fig. 11c) was higher than that of the shearing parameter combination. As high cutting stresses are produced at a higher rate of cutting speed and DOC, they specifically damage the cutting edge of the insert. As a result, the blunt insert cannot shear the abrasive fiber, and intense friction with uneven shearing produces fiber pull-out and delamination. The components machined by shearing combination through Trial 9 and 8 possess defective surface texture and non-acceptance in view of the interchangeability concept (shown in Figs[9b &11d], respectively). Therefore, to achieve a desirable surface texture in CFRP turning, it is critical to carefully consider the combined effects of the cutting parameters and the anisotropy of the material.

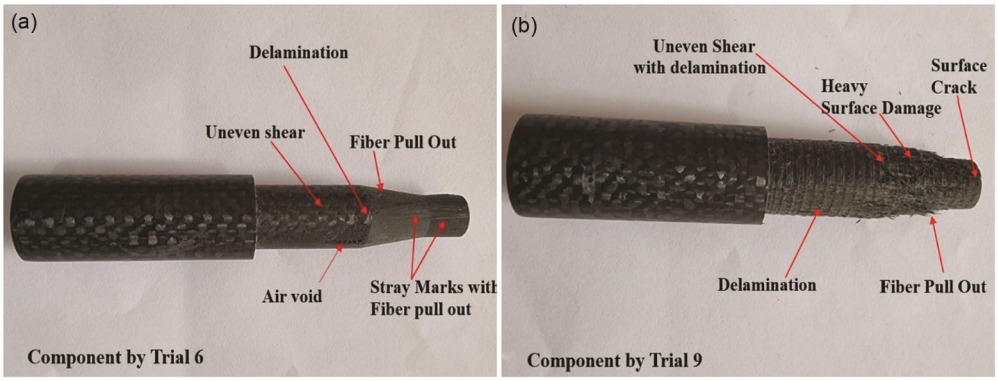

Fig. 9 — Surface texture of (a) Component by Trial 6 and (b) Component by Trial 9.

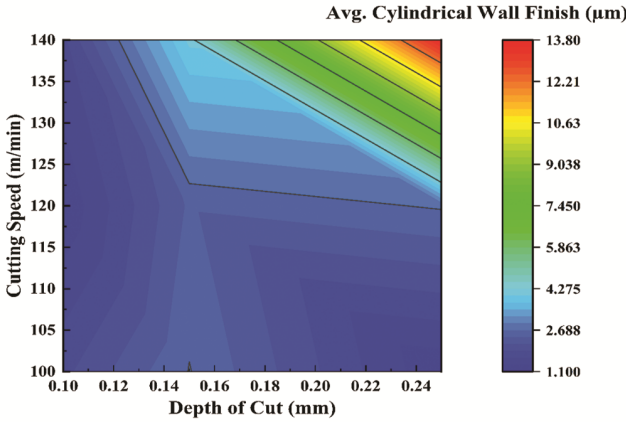

Fig. 10 — Effect of cutting speed and DOC on avg. cylindrical wall finish on components.

Therefore, understanding and managing the effects of anisotropy are critical for achieving high-quality surfaces in CFRP turning. Optimizing the cutting parameters based on fiber orientation is crucial. Strategies such as machining along the fiber direction whenever possible, using sharp tools, and controlling the cutting forces and temperatures are vital for minimizing the surface defects and achieving the desired surface finish.

3.5 Overall effect on tool wear

The 3D scatter plot (refer Fig. 12) scientifically clarifies the impact of machining parameters—cutting speed, depth of cut (DOC), and feed rate; on the progression of tool wear during CFRP turning. Every data point is a different combination of parameters, and the way they are spread out shows different wear patterns. When the cutting speed goes up from 100 to 140 m/min, crater wear gets worse because of higher thermal energy and abrasive fiber-tool interactions. Flank wear also goes up with higher feed rates (0.3 mm/rev) because there are more chip load and mechanical stress at the tool–workpiece interface. The depth of cut is also very important. Values greater than 0.15 mm increase cutting forces, which causes wear through micro-chipping and edge degradation. The plot shows that the lowest wear values are found when the cutting speed is 100 m/min, the depth of cut is 0.1 mm, and the feed is 0.1 mm/rev. This agrees with the best setting found by fuzzy AHP-GRA analysis. Figure 12 shows that process parameters have nonlinear and coupled effects on localized wear mechanisms. This shows how important it is to have precise control when machining CFRP. The graph gives empirical proof for multi-objective optimization strategies that try to improve tool life and machining consistency when coolant is used by showing how wear responses change in different parameter spaces.

3.6 Overall effect on surface quality

The 3D scatter plot shows how machining parameters affect the performance of CFRP surface finish in a scientific way (Refer Fig. 13). The three axes show cutting speed, depth of cut, and feed rate.

The dual colour coding shows the average roughness values for cylindrical and taper walls. The visualization shows that lower feed rates (0.1 mm/rev) with moderate cutting speed (100 m/min) and shallow cuts (0.1 mm) always make the surfaces smoother on both geometries. On the other hand, higher feed and depth values lead to higher roughness, which shows that the surface is becoming less stable. The plot shows that feed rate has the biggest effect on finish quality, followed by depth of cut. Cutting speed has the biggest effect on stability of results. This scientific representation proves the optimization framework by showing how refining parameters directly improves the surface finish. It stresses that precise control of feed and depth is essential for getting better taper and

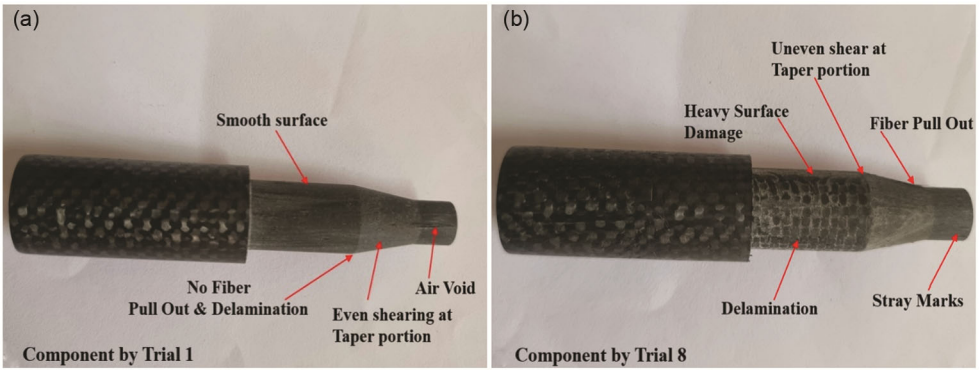

Fig. 11 — Surface texture of (a) Component by Trial 1 and (b) Component by Trial 8.

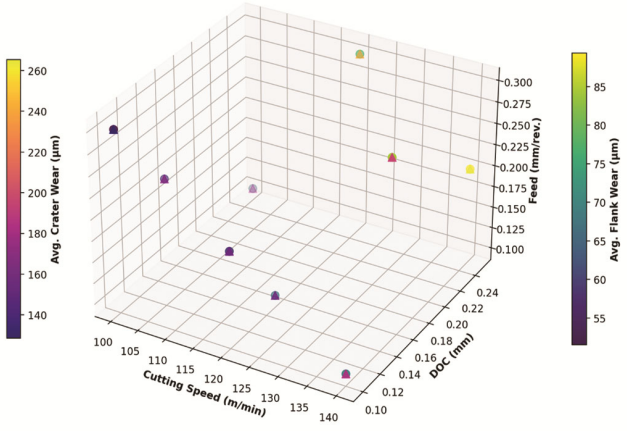

Fig. 12 — Overall effect of process parameters on cutting tool wear.

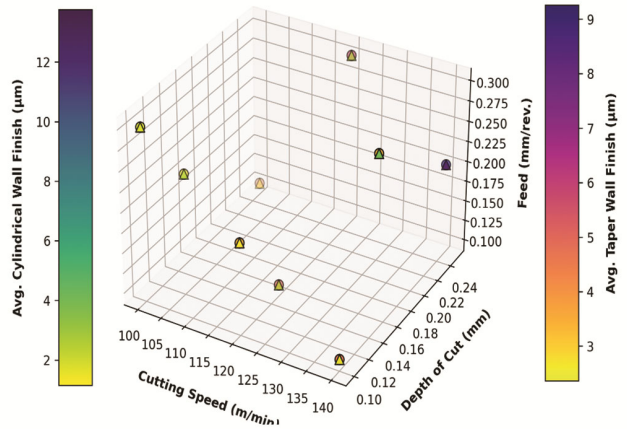

Fig. 13 — Overall effect of process parameters on surface quality of turned component.

cylindrical wall quality in CFRP machining. So, the graph clearly shows that process parameters have a nonlinear effect on surface finish. This supports the idea that iterative optimization is necessary to get the best machining performance when using coolant.

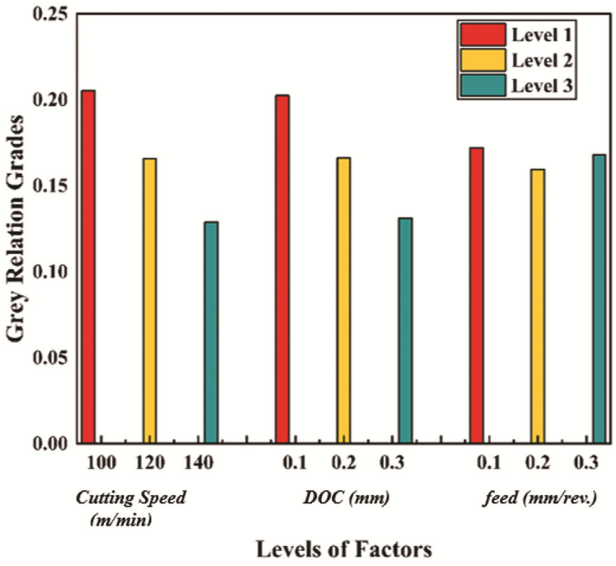

Fig. 14 — Graph of grey relational grade in the CFRP turning experimentation.

3.7 Optimum parameter setting

Fuzzy AHP GRA concluded the initial nearest optimum shearing parameters set on the basis of weights and measured performance among the conducted trials. Trial No. 1 provides the set of optimum controlled parameters (cutting speed = 100 m/min, DOC = 0.1, and Feed = 0.3 mm/rev.) with a higher grey value of 0.2436 in the present study. Now, we determine the optimum parameter setting for the anticipated results from the mean grey relational grades. Figure 14 shows the relationship between the mean GRG and parameter level used in the CFRP turning experiment.

Figure 12 illustrates that the highest mean value indicates the level of the respective process parameter for the Optimum Parameter setting, which is required to achieve the best performance output. From Table 17, the mean GRG provides an Optimum

Table 17 — Main effects on mean grey relational grades.

Factors	Mean Grey Relational Grades				
	Level 1	Level 2	Level 3	(Max-Min)	Rank
C-Cutting Speed (m/min)	0.2054	0.166	0.1288	0.0766	1
D-DOC (mm)	0.2025	0.1664	0.1312	0.0713	2
F- Feed (mm/rev.)	0.1723	0.1597	0.1681	0.0042	3
Total Mean of GRG =0.16671					

Table 18 — Predictedgrey relational grade for optimum parameters from mean grey relational grades.

Optimum Controlled Parameters from Experimental Trial				
Parameter Notation	Parameter	Level	Setting Level	GRG
C	Cutting Speed (m/min)	1		
D	DOC (mm)	1	C1D1F3	0.2436
F	Feed (mm/rev.)	3		
Required Optimum Parameters from Mean Grey Relational Grades				
C	Cutting Speed (m/min)	1		
D	DOC (mm)	1	C1D1F1	0.2523 *Predicted*
F	Feed (mm/rev.)	1		

Table 19 —Valuational experiment results.

Trial No.	Cutting Speed (m/min)	DOC (mm)	Feed (mm/rev.)	Avg. Flank Wear (µm)	Avg. Crater Wear (µm)	Avg. Taper Wall Finish (µm)	Avg. Cylindrical Wall Finish (µm)	GRG
C1D1F3	100	0.1	0.3	51.52	128.587	2.361	1.824	0.2436
C1D1F1	100	0.1	0.1	50.09	130.128	1.981	1.655	0.2523 *Predicted*

Table 20 — ANOVA result for grey relational grades.

Source	DF	Sum of Squares	Mean Squares	F	P	Status*	% Contribution
Cutting Speed (m/min)	2	0.0088	0.0044	67.22	0.015	Significant	52.43
DOC (mm)	2	0.007612	0.003806	58.12	0.017	Significant	45.34
Feed (mm/rev.)	2	0.00024	0.000122	1.87	0.349	Non-significant	1.46
Error	2	0.000131	0.000065				0.78
Total	8	0.0167					100

** $p<0.05$ is considered statistically significant*

Parameter setting for C1D1F1. Means that Cutting speed = 100 m/min, DOC = 0.1 mm, and Feed = 0.1 mm/rev.is the optimum setting parameter, which differs from the Optimum Controlled Parameters**.**

$$\hat{G} = G_t + \sum_{i=1}^{P}(G_i - G_t) \quad \ldots(12)$$

here,$\hat{G}$= GRG Predicted, G_t= GRG mean, G_i= Higher mean value of GRG predicted parameters, P=No. of Process parameters

The predicted Grey relational grade is calculated using Equation (12) [43–45]. Table 18 lists the Optimum controlled parameters from experimental trial and required optimum parameters from mean grey relational grades with the respective setting levels of the process parameters**.**

3.8 Validation test

The experimental trial was conducted by following the optimum parameters from mean grey relational grades and the performance observed after 50 component machining in view of crater wear, flank wear, cylindrical surface finish, and taper portion surface finish. Table 19 presents the details of the experimental trial.

A comparison of the performance is shown by the initial optimum controlled parameter set (C1D1F3) and the optimum setting parameter set (C1D1F1). The combination of the C1D1F1 process parameters produced a fine surface-finished component with lower tool wear than the other process parameters. Figure 15 depicts the scanning electron micrograph of the cutting insert and the image of the machined component; both show that the optimum setting parameters produce a

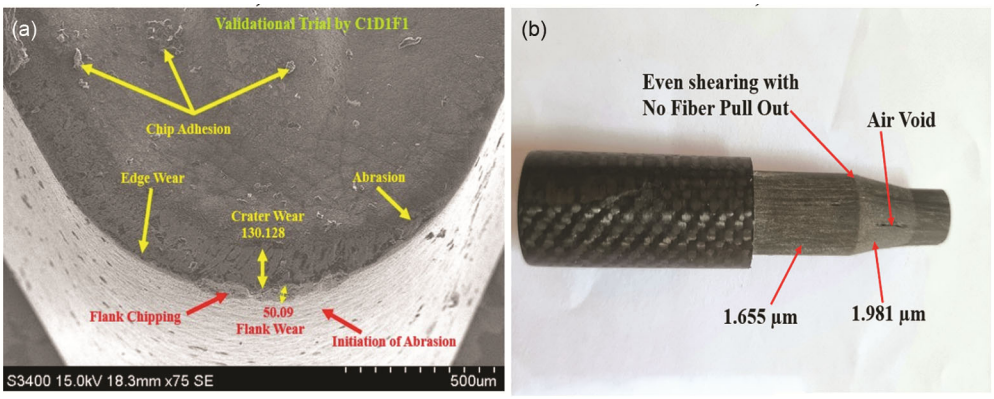

Fig. 15 — (a) SCM of cutting insert used in 50 cycle of validation trials and (b) Component by validational Trial C1D1F1.

higher performance. Thus, C1 is the cutting speed = 100 m/min, D1- Depth of Cut 0.1 mm, and F1- Feed = 0.1 mm/rev. was acceptable for CFRP turning.

3.9 ANOVA for grey relational grades

Analysis of variance (ANOVA) was used to determine which controllable parameters had a significant effect on performance characteristics. This was performed by decomposing the overall variability of the grey relational grades (computed as the total sum of squared deviations of the overall mean grey relational grade) into contributions from individual controllable parameter and error. To evaluate the effect of the variation in each controllable parameter on the performance characteristics, we used the percentage contribution of each process parameter to the overall sum of squared deviations.

Table 20 displays the results of the ANOVA corresponding to the grey relational grade values. According to the results, cutting speed, DOC, and feed contributed 52.43%, 45.34%, and 1.46%, respectively. Among these three parameters, cutting speed is the most significant parameter for multiple performance characteristics, and the grey relational grade is the most significantly affected. According to Table 19, it can be stated that the cutting speed as well as the depth of cut significantly influence the multiple performances in CFRP turning compared to the feed rate.

4 Conclusion

This study investigated the optimization of CFRP turning parameters using a combined Fuzzy AHP-GRA approach. The key conclusions are as follows:

a The integrated Fuzzy AHP-GRA approach effectively optimized the CFRP turning parameters, achieving a balance between minimizing the tool wear and maximizing the surface quality.

b The cutting speed and depth of cut emerged as the most influential parameters affecting machining performance, while the feed rate had a comparatively minor effect.

c The optimal controlled parameter setting is cutting speed of 100 m/min, depth of cut of 0.1 mm, and feed rate of 0.3 mm/rev. (C1D1F3) produced the highest Grey Relational Grade, indicating superior performance.

d A validation test using an alternate optimal combination (C1D1F1) demonstrated further improvements, including a 2.77% reduction in average flank wear, a 1.19% improvement in crater wear, a 16.09% enhancement in taper wall finish, and a 9.26% gain in cylindrical surface quality.

e SEM observations confirmed that enough coolant flow reduced resin smearing and slowed down the wear on the crater, but temperature control was still very important because localized heat buildup was seen at higher cutting speeds. The insert shape and the coolant-assisted environment work together to explain the balance between less tool wear at the best settings (100 m/min, 0.1 mm depth, 0.1 mm/rev feed) and faster degradation seen when cutting is more aggressive.

f ANOVA analysis of the Grey Relational Grade revealed that cutting speed and depth of cut contributed 52.43% and 45.34%, respectively, to overall performance, reinforcing their dominant roles in CFRP machining.

g Owing to CFRP's anisotropic nature, fiber orientation plays a significant role in machining quality. Whenever feasible, machining along the fiber direction is recommended to reduce surface defects and delamination.

Future research should explore advanced strategies such as computer-aided tool path designs for improved shearing at complex profiles, hybrid cooling methods incorporating nanoparticles to reduce tool wear and enhance finish, and comprehensive studies on cutting insert geometry and coating materials to further improve the machinability of CFRP.

Acknowledgement

The authors acknowledge the support provided by the Workshop, MET's Institute of Engineering, Bhujbal Knowledge City, Adgaon, Nashik for conducting the experiment.

References

1 Che D, Saxena I, Han P, Guo P & Ehmann K F, *J Manuf Sci Eng*, 136 (2014).
2 Demir Z, Adiyaman O & Oktay O, *Mater Test*, 61 (2019) 1109.
3 Yılmaz M, Kılınçel M &Şirin Ş, *Polym Compos*, 45 (2024) 10486.
4 Li B, Lu Z, Jin X & Zhao L, *J Intell Manuf*, 35 (2024) 2547.
5 Rajasekaran T, Palanikumar K & Vinayagam B K, *Procedia Eng*, 38 (2012) 2922.
6 Slamani M &Chatelain J-F, *Discov Mech Eng*, 2 (2023) 4.
7 Bhagwat P M, Ramachandran M & Raichurkar P, *Mater Today Proc*, 4 (2017) 7375.
8 Chen T, Liu J, Li C, Zhang J, Wang G & Li M, *Int J Adv Manuf Technol*, 129 (2023) 3933.
9 Tzotzis A, Maropoulos P & Kyratsis P, *J Intell Manuf*, (2025).
10 Sauer K, Hertel M, Fickert S, Witt M & Putz M, *Procedia CIRP*, 88 (2020) 457.
11 Li J, Xu K, Lin Z & Fu J, *Compos Part B Eng*, 283 (2024).
12 Ashworth S, Fairclough J P A, Meredith J, Takikawa Y & Kerrigan K, *Wear*, 498–499 (2022) 204340.
13 Li C, Zhao G, Ji D, Zhang G, Liu L, Zeng F & Zhao Z, *Metals (Basel)*, 14 (2024).
14 Xiao J, Gao N, Wang G, Huang P & He J, *PolymPolym Compos*, 32 (2024) 1.
15 Chen X, Zhao W, Zhao G, Jamil M & He N, *Int J Adv Manuf Technol*, 123 (2022) 1785.
16 Abdur Rob S M & Srivastava A K, *Manuf Lett*, 33 (2022) 29.
17 Fedai Y, *Processes*, 11 (2023) 1.
18 Muhamad Khairussaleh N K, Che Haron C H & Ghani J A, *J Mater Res*, 31 (2016) 1893.
19 Brouschkin A, Hintze W &Dege J H, *CIRP J Manuf Sci Technol*, 51 (2024) 201.
20 Shahruddin N S, Syazwina Mustaffa N H, Mustafa A M & Abd Halim N F H, *J Phys ConfSer*, 2051 (2021) 012054.
21 Li J, Wang C, Qiu Z, Lin Z & Fu J, *Procedia CIRP*, 131 (2025) 13.
22 Madhavan V, Lipczynski G, Lane B & Whitenton E, *J Manuf Process*, 20 (2015) 431.
23 Ge J, Fu G, Almeida J H S, Jin Y & Sun D, *Compos Struct*, 356 (2025).
24 Ge J, Luo M, Zhang D, Catalanotti G, Falzon B G, McClelland J, Higgins C, Jin Y & Sun D, *J Manuf Process*, 88 (2023) 167.
25 Zhang C, Song J, Jiang L, Gao J, Liang G, Lei C, Xie J, Wang S & Lv M, *TribolInt*, 109 (2017) 97.
26 Ozkan D, Sabri Gok M, Oge M & Cahit Karaoglanli A, *Mater Today Proc*, 11 (2019) 526.
27 Attahu C Y, Yang J, Wong K & Thein C K, *IOP Conf Ser Mater Sci Eng*, 1225 (2022) 012005.
28 Alsayed S H, Al-Salloum Y A & Almusallam T H, *Proc Inst Civ Eng Civ Eng*, 138 (2000) 131.
29 Su Y, *Compos Struct*, 220 (2019) 662.
30 Seeholzer L, Kneubühler F, Grossenbacher F & Wegener K, *Int J Adv Manuf Technol*, 115 (2021) 2905.
31 Patil A S, Sunnapwar V K, Bhole K S & More Y S, *Adv Mater Process Technol*, 8 (2022) 3706.
32 Patil A S, Sunnapwar V K, Bhole K S, Oza A D, Shinde S M & Ramesh R, *Int J Interact Des Manuf*, (2022) 1.
33 Chang D Y, *Eur J Oper Res*, 95 (1996) 649.
34 Fedai Y, *Processes*, 11 (2023) 2872.
35 Patil A, Sunnapwar V, Bhole K, Patel R, Bharambe M & Shinde S, *AIP Conf Proc*, 2985 (2024).
36 Hanish Anand S, Venkateshwaran N, Sai Prasanna Kumar J V, Kumar D, Ramesh Kumar C &Maridurai T, *Silicon*, 14 (2022) 4337.
37 Rahman A M, Rob S M A & Srivastava A K, *Procedia Manuf*, 53 (2021) 204.
38 Amrita M, Kamesh B & Leela Satya Sree K, *Mater Today Proc*, 62 (2022) 1179.
39 Patil A S, Sunnapwar V K & Bhole K S, *Int J Interact Des Manuf*, (2023) 1.
40 Patil A S, Singh D, Bhole K & Jharbade K, *J Biomater Sci Polym Ed*, 0 (2025) 1.
41 Shinde S M, Lekurwale R R, Bhole K S, Oza A D, Patil A S & Ramesh R, *Int J Interact Des Manuf*, (2022).
42 Srivastava A K & Mofakkirul Islam M, *Manuf Lett*, 41 (2024) 658.
43 Jozić S, Bajić D & Celent L, *J Clean Prod*, 100 (2015) 325.
44 Mgbemena C, Mgbemena C, Etebenumeh G & Ashiedu F, *Niger J Technol*, 35 (2016) 847.
45 Haq A N, Marimuthu P & Jeyapaul R, *Int J Adv Manuf Technol*, 37 (2008) 250.